Contents lists available at UGC-CARE

International Journal of Pharmaceutical Sciences and Drug Research

[ISSN: 0975-248X; CODEN (USA): IJPSPP]

journal home page : https://ijpsdronline.com/index.php/journal

Research article

Gabapentin Loaded Graphene Oxide Mesoporous Silica Nanocomposite: Design, Development and *In-vitro* Characterization

Ketan Patil*, Jayvadan Patel

Faculty of Pharmacy, Nootan Pharmacy College, Sankalchand Patel University, Visnagar, Gujarat, India.

ARTICLE INFO

Article history:

Received: 14 July, 2024

Revised: 08 August, 2024

Accepted: 13 August, 2024

Published: 30 September, 2024

Keywords:

Gabapentin, MSN, GO, *In-vitro*, LC-GAB-GO-MSN

DOI:

10.25004/IJPSDR.2024.160508

ABSTRACT

The present study aimed to develop lipid-coated gabapentin-loaded graphene oxide-mesoporous silica nanocomposites (LC-GAB-GO-MSN) as a novel drug delivery system. The objective was to address the poor permeability and low bioavailability issues associated with gabapentin (GAB), a BCS class III drug, by utilizing the distinctive properties of GO-MSN nanocomposites to enhance drug delivery efficiency. GAB loading within the nanocomposites was achieved through passive loading techniques, while lipid coating was carried out employing a modified thin film hydration method. Spectral characterization was conducted to determine the entrapment efficiency of GAB within the nanocomposites. Drug release studies evaluated pharmacological release kinetics developed LC-GAB-GO-MSN and GAB-GO-MSN nanocomposites. The spectral characterizations revealed an entrapment efficiency of 51.25% for GAB-MSN and 68.19% for GAB-GO-MSN. Moreover, drug release studies (*in-vitro*) demonstrated 95.70 and 70.83% drug release from LC-GAB-GO-MSN and GAB-GO-MSN nanocomposites, respectively. The design of lipid-coated LC-GAB-GO-MSN through GO-MSN incorporation followed by lipid coating offered a controlled release profile. LC-GAB-GO-MSN nanocomposites showed promise for delivering GAB and other pharmaceutical compounds with enhanced payload capacity and release kinetics, highlighting their potential advantages over current methodologies and the important role of protocells in the development of cargo delivery systems.

Introduction

Revolutionary developments in the area of nanotechnology during the last two decades have shown impressive breakthroughs and new uses in medication delivery and medicinal applications. Functionalized nanomaterials such as polymeric gold nanoparticles, dendrimers, liposomes, fullerenes, metallic NPs, assembly NPs, self-protein NPs, polymer, ferric oxide NPs, lipid, and ceramic-based NPs, etc., are included in the nanoscale drug delivery carrier for applications of biomedical and drug delivery.[1,2] Examining the relationship between biological systems and nanocomposites has become essential for determining the safety and effectiveness of medication delivery methods. When compared to traditional formulations, nanomedicine allows for less systemic cytotoxicity, increased safety, and an improvement in therapeutic efficacy at a lower dose. Among the various nanomaterials, graphene oxide-mesoporous silica nanoparticles (GO-MSN) have become the most sophisticated, cutting-edge, and popular hybrid functionalized nanocomposite materials. These nanoparticles are created by combining two distinct nanomaterials and have several appealing properties that make them efficient drug carriers.[3,4]

The GO effective conjugation with MSN expands the ultimate uses of either or both MSN and GO. Because of its porous interior, biodegradability, large surface area, adaptable pore size and diameter, biochemical stability, cargo-dig loading ability, good biocompatibility, ease of synthesis, and low cytotoxicity, GO-MSN, a highly well-liked nanomaterial in material sciences and chemistry, attracted a lot of attention and interest. The GO-MSN nanoconjugate provides the potential to precisely regulate

***Corresponding Author:** Mr. Ketan Patil

Address: Faculty of Pharmacy, Nootan Pharmacy College, Sankalchand Patel University, Visnagar, Gujarat, India.

Email ✉**:** patilktn.99@gmail.com

Tel.: +91-9923414677

Relevant conflicts of interest/financial disclosures: The authors declare that the research was conducted in the absence of any commercial or financial relationships that could be construed as a potential conflict of interest.

the distribution of a bioactive candidate to particular cells, thereby optimizing therapeutic effectiveness while reducing systemic damage to healthy tissues. The two-dimensional nanomaterial GO is a promising option for enhancing the pharmacokinetics of many medications because of its significant drug-loading ability, large surface area, and capability to permit regulated release. With its well-organized nanopores, mesoporous silica adds another level of complexity that makes it possible to precisely regulate the kinetics of drug release. Combining the benefits of GO with MSN in a nanocomposite produces a synergistic platform that can overcome the problems associated with the delivery of gabapentin (GAB).[5,6]

The structural counterpart of GABA, GAB, has been licensed for use as an adjuvant therapy for patients (>12 years) with refractory partial seizures in children, mixed seizure disorders, and partial seizures (with or without subsequent generalization).[7]

Moreover, the initiation of the GAB course commences with an administration of 300, 600, and 1800 mg/day. The administration of such high dosages frequently requires subsequent adjustments to lower doses by physicians to mitigate the risk of suicidal manifestations. Additionally, the compound demonstrated a notably reduced oral bioavailability of merely 27% alongside a biological half-life ranging from 5 to 7 hours.[8] These pharmacokinetics characteristics underscore the potential for the selection of a model drug for DDSs to enhance release patterns to overcome this problem. Research has shown that it is effective in treating many forms of neuropathic pain in both clinical and preclinical settings. GAB has been used as a first-line treatment for some neuropathic disorders, including diabetic neuropathy and peripheral neuropathy (PHN), due to its better safety profile, which includes fewer worries about medication, no interference, and interactions with the hepatic enzymes.[9]

The present study was focused on the incorporation of the bioactive substance GAB into lipid-coated GO-MSN compact sandwich-structured nanocomposites. In addition, the synthesis of GO was carried out using a modified hammering approach, at the same time as the synthesis of MSN was carried out using the sol-gel process.[10] In the current study, an approach focused on the synthesis of GO-MSN composites was optimized, taking advantage of the advantageous properties present in both GO and MSN to design materials with enhanced characteristics. [11]

This research explained the improved entrapment efficiency and drug release kinetics achieved by LC-GAB-GO-MSN nanocomposites. The current approach opened novel perspectives for protocell research by providing enhanced drug encapsulation and DDS capabilities, thereby improving therapeutic efficacy and potential, as demonstrated by the LC-GAB-GO-MSN designs.

Materials And Methods

Materials

A specimen of GAB was obtained from Shreeji Pharma International Pvt. Ltd. Vadodara, Gujarat, while Asbury Carbons, based in New Jersey, USA, supplied the graphite powder. Polylactic-co-glycolic acid (PLGA) and tetraethyl orthosilicate (TEOS) were procured from Sigma Aldrich, India. Phosphatidylcholine-90G was sourced from Lipoid GmbH, Germany, and cetyl trimethyl ammonium bromide (CTAB) procurement from Loba Chemie Pvt. Ltd., Mumbai. All substances, including solvents and chemicals, used in the experimentations were of analytical grade.

Fabrication of Mesoporous Silica Manoparticles (MSN)

Inorganic silica (untreated) was converted into stable MSN by employing CTAB as a surfactant in a one-step sol-gel process. To prevent foaming, deionized water (150 mL), CTAB (0.2 g), and diethylamine (0.5 mL) were combined in a flask and gently stirred at room temperature. The mixture was then kept at 60°C for 30 minutes to achieve the CTAB micelle's equilibrium structure. About 1-mL of TEOS was added dropwise, and the mixture was violently agitated for two hrs at 1300 rpm. After centrifuging the resultant product for 10 minutes at 10,000 rpm, excess reagents were disposed of by repeatedly washing them in ethanol. Overnight drying was done on the collected residue. [12]

Fabrication of Graphene Oxide (GO)

Graphene oxide (GO) was prepared to utilize the Hummers method with a modification. Initially, 3.0 g of graphite powder was combined with 70 mL of conc. Additionally, H_2SO_4 is stirred while kept in an ice bath The suspension's temperature was carefully maintained below 10°C during the process. Afterward, 9.0 g of $KMnO_4$ was added slowly to the mixture while ensuring continuous vigorous agitation, leading to the transformation of the suspension into the viscous slurry. The reaction mixture was maintained below 10°C for an interval of 120 hours. Resulting, the system was transferred to a 40°C oil bath and underwent rigorous stirring for approximately 60 minutes. Subsequently, 150 mL of distilled water was poured, and the solution was agitated at 95°C for 15 minutes. Further, 500 mL of distilled water was introduced, by the slowly added 15 mL of H_2O_2 (30%), and the observed result was a clear transformation in color, shifting from dark brown to yellow. Centrifugation at 5000 rpm for 5 minutes effectively separated the suspension into supernatant liquor and a golden-colored residue. The supernatant was subjected to additional centrifugation at 15000 rpm for 5 minutes to eliminate any remaining suspended substances. The resulting precipitates were then ultrasonicated, collected, and dried in a vacuum oven at 60°C.[13]

Fabrication of GO-MSN Manocomposite

The hybrid GO-MSN nanocomposite was effectively synthesized by suspending 120 mg GO add an aqueous solution comprising 4 g CTAB in 150 mL of distilled water. The GO-MSN nanocomposite was synthesized by the technique described by Zhou *et al*., (2012). [14] After another 180 minutes of ultrasonication, stirring was applied to the reaction mixture continuously for 2 hours at 40°C. Afterward, 4 mL of TEOS was dropwise added to the mixture and agitated for 12 hours. After centrifuging the reaction mixture again to separate the precipitate, deionized water was used for washing. To create the GO-MSN product, the final compound was dried out at room temperature.

Preparation of GAB-MSN and GAB-GO-MSN Nanocomposites

The outer surface of both GO-MSN and MSN nanocomposites underwent activation through heating to 60°C for 1-hour, aimed at eliminating any residual moisture. Subsequently, 100 mg of MSN and GO-MSN nanocomposites were immersed in a phosphate buffer solution. at pH 6.8 containing GAB at a conc. of 1-mg/mL. The composite was continuously stirred for 24 hours. Assessment of the efficient absorption and functionalization of GAB on the surfaces of GO-MSN and MSN nanocomposites was conducted utilizing UV-vis spectroscopy. [15]

Preparation of Loaded with GAB Lipid Bilayer on MSN and GO-MSN (LC- GAB -MSN, LC- GAB-GO-MSN)

The synthesis of lipid-coated GAB-MSN and GAB-GO-MSN nanocomposites was efficiently accomplished utilizing a modified thin film hydration technique. Initially, (7.5 mg) PLGA, (15 mg) of phospholipion 90 G, and (7.5 mg) of soybean lecithin was dissolved in (15 mL) chloroform. Subsequently, a mixture having 60 mg of GO-MSN nanocomposite and pre-distributed GAB-MSN was subjected to ultrasonic treatment for 10 minutes. Evaporation of the solvent under reduced pressure was conducted using a rotary vacuum evaporator, producing a thinner layer. Throughout this phase, the lipids and PLGA occurred on the surface of both MSN and GO-MSN. As a result, the film formed once again suspended in phosphate buffer with a pH of 7.4, and vigorously shaken on an orbital shaker for a duration of 3 hours. The resuspended sample underwent centrifugation for 10 minutes at 5000 rpm to isolate the lipid. [16]

Synthesized GO, MSN, and GAB-GO-MSN Characterisation

Primary identification of the synthesized GO-MSN and intermediates was done using FT-IR spectroscopy (FTIR-8200, Delhi, India). Spectra (Diffuse reflectance) was used to disperse the material using the KBr (1:100) ratio and scan the area between 4000 and 400 cm to acquire the FTIR spectrum. The drug content and entrapment efficiency of GAB-GOMSN and GAB-MSN were determined by UV-vis spectroscopic (UV1800, Japan). An additional helpful tool for figuring out the *in-vitro* release of GAB pattern from manufactured components was the UV-vis spectrum. Utilizing DSC (DSC 821e Mettler Toledo, Switzerland), the sample's temperature variations were recorded. The polydispersity index, particle size, and zeta potential were determined at a backscatter angle of 1800 without dilution using the NanoPlus 3 Particulate System from Micrometrics in the USA.

Results And Discussion

FTIR analysis

The FTIR spectrum of gabapentin, depicted in Fig. 1(A), revealed a peak at 1626 cm^{-1} for NH stretching and 1436 cm^{-1} for NH bending. As it is a zwitterion in its solid state, there is usually no peak seen in the 3500 to 3300 cm^{-1} region. The two peaks found at 2932 and 2861 cm^{-1} was associated with $-NH_3+$ stretching vibrations. Furthermore, CH and C = O stretching are responsible for the maxima at 2921.16 and 1391.83 cm^{-1}, correspondingly. Moreover, the ionized asymmetric carboxylate group and NH_{3+} deformation is responsible for vibrations detected at 1546 and 1621 cm^{-1}, correspondingly. The distinct peaks at 1319.82 and 1918.21 cm^{-1} is attributed to C-O and CN stretching, respectively. These results are consistent with a prior study. [17-19] Fig. 1(B) exhibits typical peaks from the synthesized MSN. The Si-OH stretching vibration is linked to the wide band at 3464 cm^{-1}. Proceeding to the FTIR spectrum of the synthesized GO shown in Fig. 1(C), the high-frequency region shows a wide peak that stretches from 3000 to 3700 cm^{-1} and a specific peak at 1628 cm^{-1}, Attributed to the stretching and bending vibrational modes of OH groups, which are due to the adsorption of water molecules on graphene oxide. This observation indicates that the sample has significant hydrophilicity. The existence of oxygen functional groups was verified by a peak at 1047 cm^{-1}, which is suggestive of the C = O bond. There are other observed peaks at 1234 cm^{-1} (C-O

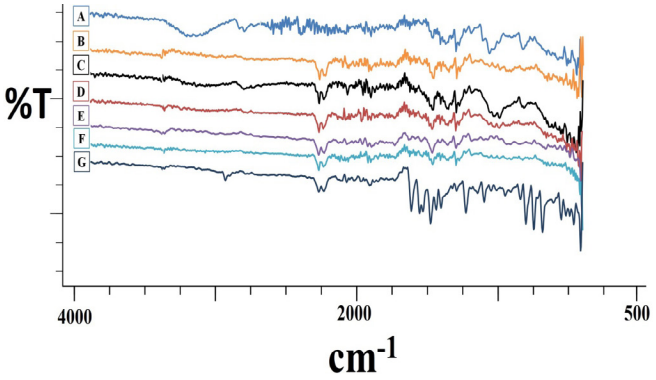

Fig. 1: FTIR spectrum of (A) GAB, (B) MSN, (C) GO, (D) GO-MSN, (E) GAB-MSN, (F) GAB-GO-MSN, (G) LC-GAB-GO-MSN

stretch) and 1645 cm^{-1} (C = C). Fig. 1(D) FTIR spectra show absorption peaks at 3400 and 2920 cm^{-1}, which support the usual C-H and OH stretching and point to the existence of GO and MSN. Peaks at 795 and 1068 cm^{-1}, which are indicative of Si-O and C-O stretching, respectively, validate the nanocomposite's effective linking and are in line with previous research. The successful loading of GAB onto MSN was confirmed by GAB-loaded MSN FTIR spectra, which displayed 2846 and 3268 cm^{-1} absorption peaks (Fig. 1(E)). Peaks at 1325 and 901 cm^{-1} verify the GAB successful loading inside the MSN porous structure, whereas peaks at 1548 and 1716 cm^{-1} are attributable to NH bending and C = O stretching, revealing the typical peaks of GAB. The GAB-loaded GO-MSN nanocomposite's FTIR spectra in Fig. 1(F) show peaks at 3425 and 2728 cm^{-1} which correspond to NH and C-H stretching. The band that emerged confirms the existence of GO and shows that GAB was successfully loaded onto the external surface. The results demonstrate that GO-MSN has an amine group, indicating that GAB has been successfully loaded onto the MSN nanoconjugate. The FTIR spectra of GAB-loaded GO-MSN coated with lipids are shown in Fig. 1(G), with NH and CH stretching-related peaks at 3217 and 2865 cm^{-1}. Peaks at 1602 and 1658 cm^{-1} are linked to NH bending and C = O stretching.

Characterization of Particle Size and Zeta Potential

Since the body's defense mechanisms need to be able to detect and reject nanoparticles, their size and surface charge have a significant impact on what happens to them after injection. The surface charge, also known as the zeta potential, is one significant component affecting the stability of the NPs. Particles with larger negative or positive zeta potential values develop greater repulsive forces. The synthesized MSN, which was measured by dynamic light scattering, had a polydispersity index (PDI) of 0.312 and a particle size of 453 nm. At 10.51 mV, the zeta potential was recorded (Fig. 2A, B). The smallest particle size shows better particle packing and shows that the synthesis technique for getting MSN was successfully implemented. In the present investigation, there was a small increase in size due to the immersion of two or more components during the production of the nanocomposite. With a PDI of 0.350 and a positive potential of 11.52 mV, the GO the average (mean) particle size was measured to be 514 nm, indicating the improved technique promotes favorable interactions leading to GO development (Fig. 2(C, D)). The GO-MSN representation in Fig. 2(E, F) showed a rise from 0.341 to 0.367 in PDI, which was statistically significant along with a change in the value of GO zeta potential, which is attributable to the GO-MSN conjugation ($p < 0.01$). This rise in PDI and particle size is consistent with earlier findings on MSN. Similarly, drug-loaded GO-MSN Fig. 2 (G, H) displayed a similar pattern, with the reported findings attributable to the binding of GAB and a consequent drop in zeta potential to -27.88 mV. It is an important factor in cellular connection since it favors

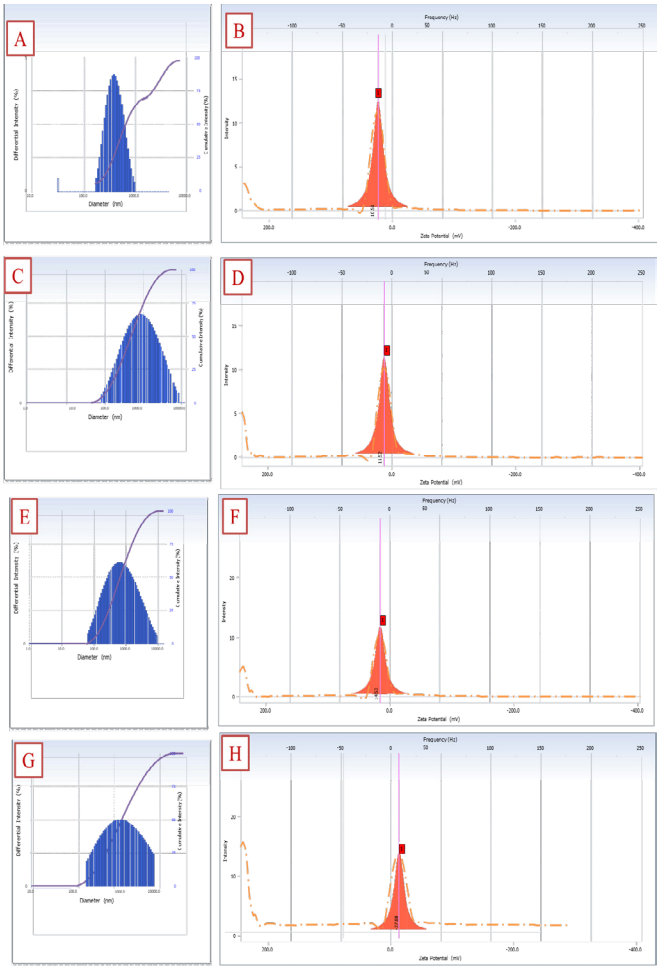

Fig. 2: Zeta potential and particle size of (A, B) MSN, (C, D) GO, (E, F) GO-MSN, (G, H) GAB-GO-MSN

positive charge. However, because of the weak charge on the cell membrane, at GO-MSN, a negative charge may affect this interaction. The lipid-coated structures have increased the size of GO-MSN might have been caused by the incorporation of the drug that was loaded into the GO-MSN conjugate, which increased the pore volume and surface area. SEM analysis revealed that the drug-loaded, lipid-coated GO-MSN had a spherical shape, increasing its surface area for environmental interaction. Because phospholipids in cells may be neutral or negatively charged, endocytosis may play a role in the absorption of GO inside cells instead of only the direct interaction between phospholipids and GO.[10] These results are in line with other research findings.

DSC Study

The drug-carrier interaction was confirmed by the DSC thermogram (Fig. 3). Based on Fig. 3(A), the MP (melting point) of GAB is shown by the prominent endothermic peak at 164°C. The drug material was present in the amorphous form in the matrix consisting of crystalline lactose and microcrystalline cellulose, as shown by

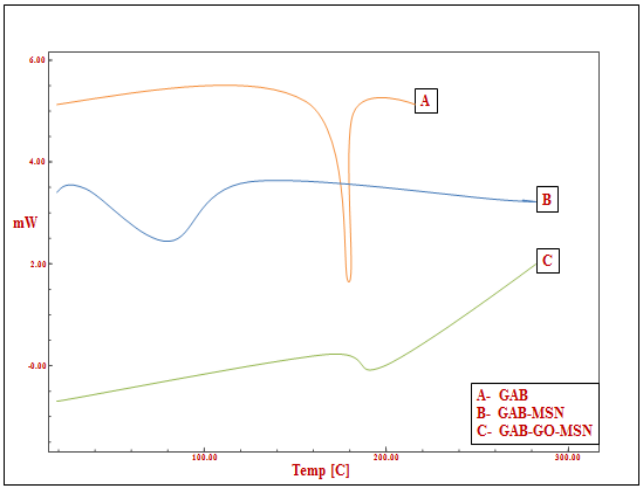

Fig. 3: DSC thermogram of (A) GAB, (B) GAB-MSN and (C) GAB-GO-MSN

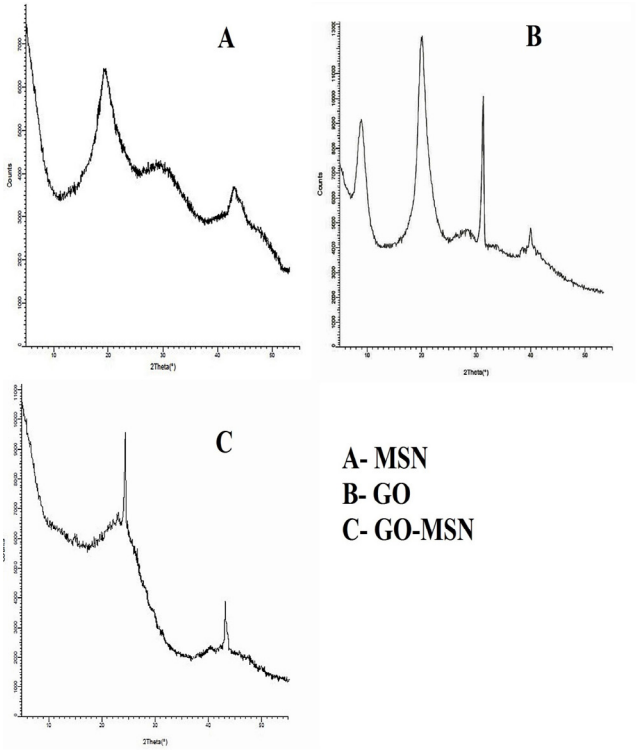

Fig. 4: XRD of synthesized (A) MSN (B) GO (C) GO-MSN

the lack of an endothermic peak of GAB caused by the melting of crystalline GAB present in the drug-loaded extrudates. The DSC thermogram of the GAB-loaded MSN is shown in Fig. 3(B), where temperature is plotted against weight loss. The findings demonstrate that GAB is equally disseminated inside the pores of MSN, residing in a noncrystalline condition, which is clear from the lack of a GAB endotherm in Fig. 3(B). Furthermore, the research showed a peak at 85°C, which was linked to the first water loss and the presence of surfactant chains, which had a wider stability range up to 200°C. The DSC thermogram of GAB-loaded GO-MSN, presented in Fig. 3(C), exhibited a minor endothermic peak at 168.0°C. This indicated that some GAB was covalently bonded to the substrate surface, thereby enhancing stability compared to free GAB molecules. Additionally, this suggested that a greater number of GO-MSN carriers were available for the adsorption of GAB, resulting in an increased dispersion of GAB into the GO-MSN conjugate.

XRD Analysis

The purpose of the X-ray diffraction investigation was to find out whether the nanocomposite was amorphous or crystalline. Every sample showed a wider diffraction at a 2θ value of the around 21° and a smaller reflection centered at about 31°, which matched the diffraction of the 100 and 110 facets of a C structure that was comparable to graphite. The 2D order, which exhibits a hexagonal pore arrangement with centered and primitive cubic structures (Fig. 4(A)), study illustrates the crystalline structure of MSN. In Fig. 4(B), the XRD peak of GO shows peaks at 12, 18, 33, and 43.10°, which correspond to the lattice planes (100), (210), and (300, 221). These peaks suggest that the structure of the carbon is hexagonal, with primitive cubic and centered cubic (110) structures. In line with earlier findings, these peaks also imply the graphite sheets which is oxidation and the advancement of sheets of GO. Moreover, in agreement with the literature, the "d spacing at (0.73), (0.42), (0.24), and (0.17)" shows a decrease in the size of graphene sheets, which may result in interlayer spacing. The results showed a notable peak at 11°, which is representative of a typical diffraction peak of GO. Fig. 4(C) shows that as GO is oxidized and changes to the graphite, the peak of XRD of GO vanishes, and a novel peak forms at 23.9°, suggesting the successful reduction of GO, similar to prior results.[20] Strong peaks at 24.8° and 44.8°, attributable to the carbon lattice planes (100) and (110), are seen in the synthesized GO-MSN's X-ray diffraction pattern, showing body-centered and hexagonal primitive cubic structures with d spacing of (0.31) and (0.17). The information shows that the GO intensity peak has decreased and that GO-MSN particles have formed a multilayer structure. As seen in the XRD pattern, the nanoparticles themselves also have somewhat uneven surfaces as opposed to entirely smooth ones. Moreover, attention should be given to the anticipated trenches and interstitial gaps between neighboring nanoparticles.

Raman Analysis

Raman spectroscopy, which uses the D as well as G peaks and their implications as distinguishing features, the study gathers structural information on carbon-based materials by employing a non-destructive technique often in use. The G-band in Fig. 5 is defined as the center of the two primary spectra of GO and GO-MSN, which are centered at about

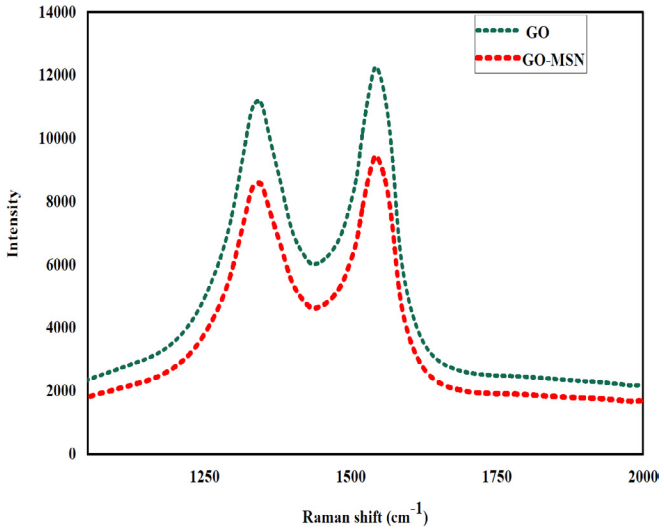

Fig. 5: Raman spectra of GO and GO-MSN

1604 and 1599 cm, respectively. This band is thought to be caused by the hexagonal rings' stretching vibrations, which give graphite its crystalline structure. The D-peak, or breathing vibration of sp^2 hybridized carbon rings, is shown by the peaks at 1358 and 1348 cm^{-1}. Stretching sp^2 carbon rings and chains lead to the culmination of the G peak, which coincides with the interior of the Brillouin zone of optical Eg phonons. As the breathing oscillation of aromatic rings, the D peak represents sample defects. Faults are usually estimated using the intensity ratio between ID/IG; a larger ratio indicates more faults and a lower degree of graphitization. Because graphene oxide is present, the ID/IG intensity ratio for both GO and GO-MSN was 0.85, suggesting a crystalline composition. This validates the production of graphene oxide with excellent crystallinity and purity and predicts a higher degree of order and less deformation. It also broadens edge planes and the degree of irregularity in graphene sheets. These outcomes align with previously published data.

Scanning Electron Microscopy

At various magnifications, the surface morphology of the nanoconjugates was observed with scanning electron microscopy (SEM). Agglomerated MSN with spherical particles and a rough surface may be seen in Figs 6(A, B). The agglomerates were produced by hydrolyzing and polymerizing precursors into small, well-organized particles, a process known as polycondensation. Interlinking polymerization was the method via which final aggregates were formed. Micrographs of produced GO in Figs 6(C, D) showed the two-dimensional sheet-like structure of GO produced using a modified Hummers technique. These pictures unequivocally show that GO is arranged in numerous lamellar layers, with distinct borders for each sheet. A layered structure may be seen in stacked films, which display sections with pronounced

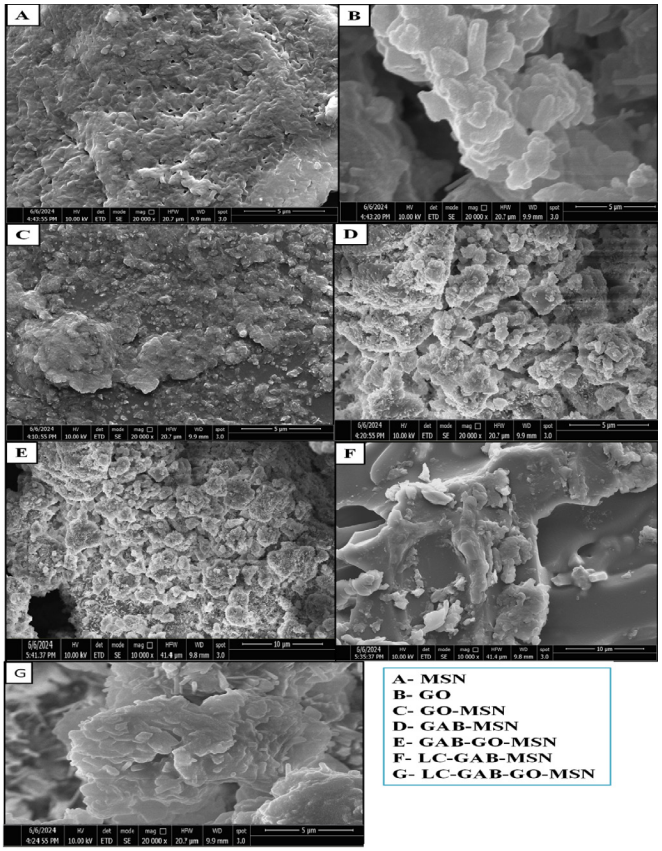

Fig. 6: SEM images of synthesized (A) MSN, (B) GO, (C) GO-MSN (D) GAB-MSN, (E) GAB -GO-MSN, (F) LC- GAB - MSN, (G) LC- GAB-GO-MSN

wrinkles. Lamellar structures measuring 239 µm in width and up to 1.29 mm in length are seen in the SEM images. Because of the insertion of functional groups containing oxygen, individual graphene oxide (GO) sheets, which are 1 to 2 µm thick, the dimensions are significantly larger than the thickness of a monolayer of graphene. The GO sheets are particularly thicker toward the borders, which is explained by the number of functional groups that contain oxygen there. The SEM images of artificial GO-MSN were shown in Figs 6 (E, F), which demonstrated a luminous structure of GO with compatible and very thin films possessing a continuous folded layered structure. This discovery is consistent with earlier research showing that material contraction during heat treatment causes a significant number of sheets to get rumpled and enhances the rough surface. The effective synthesis of GO with extracted graphene sheets using silica as a smooth dispersion was confirmed by the observation of silica particles accumulating in graphene sheets. The full dispersion of GAB in the mesoporous structure of silica nanoparticles is responsible for the observed broad spread of GAB-loaded MSN, with the clusters covering the entire surface. Lipid-coated GAB-loaded mesoporous silica nanoparticles are enclosed on the porous surface in Figs 6(E, F), preventing direct exocytosis and shielding GAB from endogenous

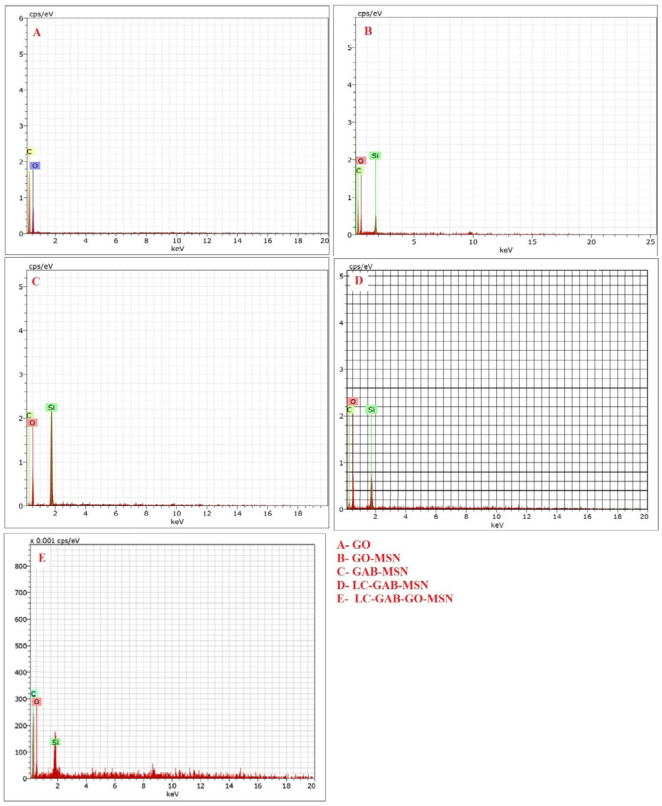

Fig. 7: Elemental analysis of (A) GO, (B) GO-MSN (C) GAB-MSN, (D) LC- GAB - MSN, (E) LC- GAB-GO-MSN

degradation. GAB-loaded MSN surface morphology is visible; it has a smooth surface with a diameter that ranges from 500 nm to 3 µm. GO-MSN, which shows drug encapsulation between MSN spores and exfoliated GO, is shown in Figs 6(C, D). The GO-MSN displays a broad range of sizes from 500 nm to 1 µm, indicating a greater quantity of GO-like nanosheets stacked in loosely packed layered nanosheets. Figs 6(E, F) show the GAB-loaded GO-MSN with an amorphous GO-silica nanocomposite, which has a size range of at least 3.00 to 5.00 µm. The picture of SEM reveals the synthesized GAB-GO-MSN in both a bi-continuous and particulate form. Particles that seem to separate from one another's masses suggest that the sample has become smoother and that exfoliation-folded graphene oxide sheets are easily visible. The existence of a lipid bilayer, or what are known as protocells in targeted drug delivery systems, is suggested by this smoothing in particle shape.

Elemental Analysis

Fig. 7 shows the element concentrations of the produced nanocomposite as determined by elemental analysis using energy-dispersive X-ray spectroscopy (EDX). In Fig. 7(A), the EDX spectrum displays the elemental arrangement of the synthesized material, demonstrating the presence of carbon (C) at 63.15% and oxygen (O) at 38.54%. Thanks to the material's beneficial effects from hydroxyl and carboxylic groups, the concentration of oxygen has

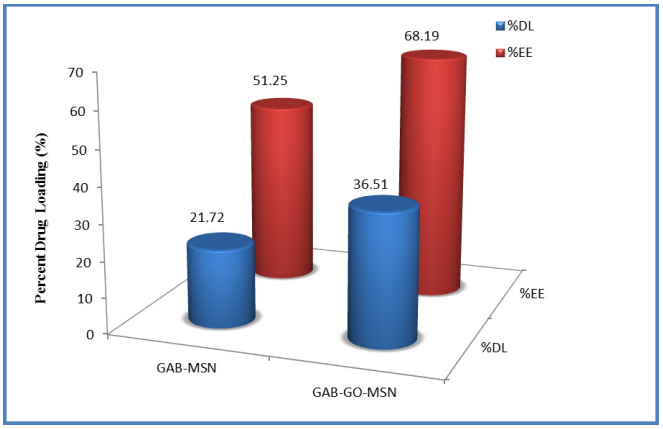

Fig. 8: Drug loading and entrapment efficiency of MSN and GO-MSN

increased. The elemental analysis of the synthesized GO-MSN is shown in Fig. 7(B), where silicon (Si), C, and O are present. The claim that there are no discernible impurities after the lack of additional elements supports calcination. Functionalization is confirmed by the drop in oxygen content, which shows that the silica incorporated during synthesis has been replaced. It is discovered that the atomic weight percentages of C are 61.10%, O 36.45%, and Si 2.22% for GO-MSN. Moreover, as indicated by Fig. 7(C), the elemental analysis of ACV-MSN confirms the presence of C (22.30%), O (56.29%), and Si (24.41%) during the synthesis of GO-MSN. Additionally, Fig. 7(D) demonstrates the elemental mapping of LC-ACV-MSN, depicting the presence of C (40.01%), O (53.29%), and Si (7.50%). The presence of C at 66.32%, O at 30.55%, and in Fig. 7(E) of the EDX spectrum, a low quantity of Si of GAB-loaded GO-MSN indicates that the synthesis of GAB-loaded GO-MSN was successful. Overall, the EDX analysis confirms the existence of certain elements in each material and supports the effective synthesis and functionalization processes by offering insight into the elemental composition of the generated nanocomposites.

Percentage Entrapment Efficiency and Percent Drug Loading

The investigation concentrated on GAB-loaded MSN as well as GO-MSN nanocomposites to ascertain the effectiveness of entrapment, as shown in Fig. 8. The major goal was to develop a technique for molecularly encapsulating GAB on the surfaces of MSN and GO-MSN to achieve high loading efficiency. Afterwards, incorporating GAB onto "MSN and GO-MSN" nanocomposites, the loading of GAB was carried out. The determined efficiency of entrapment was 51.25% for GAB-MSN and 68.19% for GO-MSN nanocomposite. Furthermore, it was found that the GAB in MSN and GO-MSN loading efficiency was 21.72% and 36.51%, respectively. When GO-MSN was used, the loading percentage of GAB rose dramatically, peaking at 36.51%. This implies that electrostatic interactions between GAB and GO-MSN caused the increased loading of GAB.

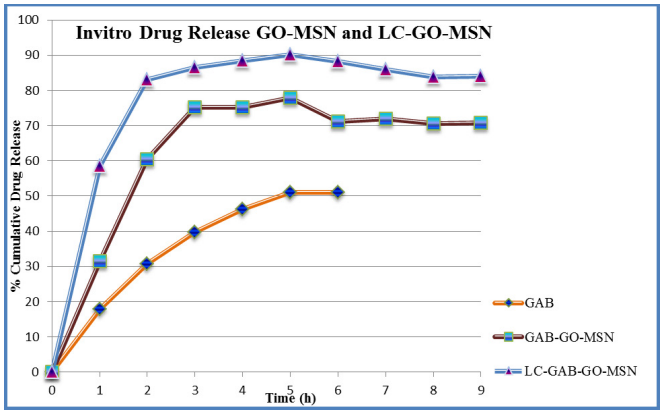

Fig. 9: *In vitro* GAB release

Examination of Drug Release under *in-vitro* Conditions

The corresponding kinetics of *in-vitro* release for the developed nanocomposite is shown in Fig. 9. The release profile indicates that pure GAB exhibited a release ranging from 40 to 52% within a mere 6 hours. Conversely, LC-GAB-GO-MSN demonstrated a substantially higher release of 95.70%, while the designed GAB-GO-MSN exhibited a release of 70.83%.

The analysis of the release pattern underscores the stability of GAB in PBS and suggests that the rapid release of GAB stems from the combined effect of the base shift induced by the LC-GAB-GO-MSN nanocomposite. Furthermore, the collected data support a dual-factor mechanism in which the disruption of the lipid layer and the electrostatic interactions between GAB-GO-MSN play an important role in controlling the release of GAB. Coating with the lipid layer results in an augmented release of GAB.

Conclusion

In conclusion, the design, development, and *in-vitro* characterization of the LC-GAB-GO-MSN nanocomposites denoted a notable advancement in the field of DDS. The synergistic amalgamation of GO and MSN not only amplifies the loading efficiency of GAB but also facilitates controlled release kinetics. Analytical techniques such as FTIR, EDX, and release assays substantiate the exceptional fabrication and characterization of the nanocomposites, underscoring its potential for efficacious drug delivery. The findings underscore the significance of electrostatic interactions and lipid layer dissociation in governing GAB release kinetics. Future research endeavors should focus on refining the composition for precise dosage control and elucidating the nanocomposites' functionality *in-vitro*, thus offering promising avenues for therapeutic applications. The incorporation of a lipid-encapsulated carrier aids in establishing an optimal local concentration by facilitating the sustained release of GAB at a controlled rate. Consequently, the synthetic LC-GAB-GO-MSN manifests distinctive and promising attributes that can be harnessed across diverse applications. In summary, our experiments present notable advantages over conventional methods, enhancing the release profile of GAB drug delivery systems through the exploration of protocells as cargo carriers.

Acknowledgment

In this study, the researchers extend their gratitude to HRPIPER Shipur for the provision of critical facilities, which played a significant role in the successful execution of their research activities.

References

1. Thi TTH, Nguyen TNQ, Hoang DT, Nguyen DH. Functionalized mesoporous silica nanoparticles and biomedical applications. Materials Science and Engineering: C. 2019;99:631-56. Available from: https://doi.org/ 10.1016/j.msec.2019.01.129
2. Thi TTN, Tran TV, Tran NQ, Nguyen CK, Nguyen DH. Hierarchical self-assembly of heparin-PEG end-capped porous silica as a redox sensitive nanocarrier for doxorubicin delivery. Materials Science and Engineering: C. 2017;70:947-54. Available from: https://doi.org/10.1016/j.msec.2016.04.085
3. Wang Z-M, Wang W, Coombs N, Soheilnia N, Ozin GA. Graphene oxide– periodic mesoporous silica sandwich nanocomposites with vertically oriented channels. Acs Nano. 2010;4(12):7437-50. Available from: https://doi.org/10.1021/nn102618n
4. Wang Y, Wang K, Zhao J, Liu X, Bu J, Yan X, *et al.* Multifunctional mesoporous silica-coated graphene nanosheet used for chemo-photothermal synergistic targeted therapy of glioma. Journal of the American Chemical Society. 2013;135(12):4799-804. Available from: https://doi.org/10.1021/ja312221g
5. Kuila T, Bose S, Mishra AK, Khanra P, Kim NH, Lee JH. Chemical functionalization of graphene and its applications. Progress in Materials Science. 2012;57(7):1061-105. Available from: https://doi.org/10.1016/j.pmatsci.2012.03.002
6. Gao W. Graphene Oxide: Reduction Recipes, Spectroscopy, and Applications. Springer. 2015:61-95. Available from: https://doi.org/10.1007/978-3-319-15500-5
7. Honarmand A, Safavi M, Zare M. Gabapentin: an update of its pharmacological properties and therapeutic use in epilepsy. Journal of Research in Medical Sciences. 2011;16(8):1062-9.
8. Dembla NM, Maniyam AP, Agarwal SJP, Journal PI. Formulation development and evaluation of gabapentin controlled release tablets. 2015;2(3):00021. Pharmacy and Pharmacology International Journal Available from: https://doi.org/10.15406/ppij.2015.02.00021
9. Vranken JH. Mechanisms and treatment of neuropathic pain. Central Nervous System Agents in Medicinal Chemistry. 2009;9(1):71-8. Available from: https://doi.org/10.2174/187152409787601932
10. Patil KB, Patel JK, Goswami HH, Chaudhari AS. Engineering. Design of Surface Modified Acyclovir-loaded Graphene Oxide–Mesoporous Silica Nanocomposite: Optimization and In Vitro Characterization. Nano Biomedicine and Engineering. 2024. Available from: https://doi.org/10.26599/NBE.2024.9290076
11. Deshmukh PK, Lakade SH, Jaiswal UR, Harde MT, More MP. One step synthesis approach of mesoporous silica packed with graphene oxide nanosheet: Characterisation and drug release aspects. Materials Technology. 2022;37(11):1677-90. Available from: https://doi.org/10.1080/10667857.2021.1972689
12. Han L, Zhou Y, He T, Song G, Wu F, Jiang F, *et al.* One-pot morphology-controlled synthesis of various shaped mesoporous silica nanoparticles. Journal of materials science. 2013;48:5718-26. Available from: https://doi.org/10.1007/s10853-013-7501-8
13. Farghali MA, Abo-Aly MM, Salaheldin TA. Modified mesoporous zeolite-A/reduced graphene oxide nanocomposite for dual removal of methylene blue and Pb^{2+} ions from wastewater. Inorganic Chemistry Communications. 2021;126:108487. Available from:

https://doi.org/10.1016/j.inoche.2021.108487
14. Zhou M, Li X, Cui J, Liu T, Cai T, Zhang H, *et al*. Synthesis and capacitive performances of graphene/N-doping porous carbon composite with high nitrogen content and two-dimensional nanoarchitecture. International Journal of Electrochemical Science. 2012;7(10):9984-96. Available from: https://doi.org/10.1016/S1452-3981(23)16252-3
15. Dalagan JQ, Enriquez EP. One-step synthesis of mesoporous silica–graphene composites by simultaneous hydrothermal coupling and reduction of graphene oxide. Bulletin of Materials Science 2014;37:589-95. Available from: https://doi.org/10.1007/s12034-014-0661-6
16. Han N, Zhao Q, Wan L, Wang Y, Gao Y, Wang P, *et al*. Hybrid lipid-capped mesoporous silica for stimuli-responsive drug release and overcoming multidrug resistance. ACS applied materials & interfaces. 2015;7(5):3342-51. Available from: https://doi.org/10.1021/am5082793
17. Dinesh Y, Chunara H, Panchal H. Formulation development and evaluation of gabapentin immediate release tablets. Journal of Emerging Technologies and Innovative Research. 2021; 8(5):c418-c428.
18. Rimawi IB, Muqedi RH, Kanaze FI. Development of Gabapentin Expandable Gastroretentive Controlled Drug Delivery System. Sci Rep. 2019 Aug 12;9(1):11675. Available from: https://doi.org/10.1038/s41598-019-48260-8
19. Hsu CH, Ke WT, Lin SY. Progressive steps of polymorphic transformation of gabapentin polymorphs studied by hot-stage FTIR microspectroscopy. J Pharm Pharm Sci. 2010;13(1):67-77. Available from: https://doi.org/10.18433/J3FS32
20. Minh Dat N, Linh VNP, Phuong NTL, Quan LN, Huong NT, Huy LA, *et al*. The effects of concentration, contact time, and pH value on antibacterial activity of silver nanoparticles decorated reduced graphene oxide. Materials Technology. 2019;34(13):792-9. Available from: https://doi.org/10.1080/10667857.2019.1630898

HOW TO CITE THIS ARTICLE: Patil K, Patel J. Gabapentin Loaded Graphene Oxide Mesoporous Silica Nanocomposite: Design, Development and *In-vitro* Characterization. Int. J. Pharm. Sci. Drug Res. 2024;16(5):804-812. **DOI:** 10.25004/IJPSDR.2024.160508